Applied Physics Letters

Impact of Sulfur on the melt dynamics of glass forming $Ti_{75}Ni_{25-x}S_x$

Cite as: Appl. Phys. Lett. **117**, 013702 (2020); https://doi.org/10.1063/5.0012409
Submitted: 05 May 2020 . Accepted: 23 June 2020 . Published Online: 07 July 2020

J. Wilden, F. Yang, D. Holland-Moritz, S. Szabó, W. Lohstroh, B. Bochtler, R. Busch, and A. Meyer

Applied Physics Letters ARTICLE scitation.org/journal/apl

Impact of Sulfur on the melt dynamics of glass forming $Ti_{75}Ni_{25-x}S_x$

Cite as: Appl. Phys. Lett. **117**, 013702 (2020); doi: 10.1063/5.0012409
Submitted: 5 May 2020 · Accepted: 23 June 2020 ·
Published Online: 7 July 2020

View Online Export Citation CrossMark

J. Wilden,[1,a)] F. Yang,[1] D. Holland-Moritz,[1] S. Szabó,[1,2] W. Lohstroh,[2] B. Bochtler,[3] R. Busch,[3] and A. Meyer[1]

AFFILIATIONS

[1]Institut für Materialphysik im Weltraum, Deutsches Zentrum für Luft- und Raumfahrt (DLR), 51170 Köln, Germany
[2]Heinz Maier-Leibnitz Zentrum (MLZ), Technische Universität München, 85747 Garching, Germany
[3]Lehrstuhl für metallische Werkstoffe, Universität des Saarlandes, 66123 Saarbrücken, Germany

[a)]Author to whom correspondence should be addressed: johanna.wilden@dlr.de

ABSTRACT

Substitution of Nickel by Sulfur leads to bulk metallic glass formation in eutectic $Ti_{75}Ni_{25}$. In order to understand the improved glass forming ability, a detailed analysis of the melt dynamics was performed. We measured the density, the viscosity, and the self-diffusion of $Ti_{75}Ni_{25-x}S_x$ ($x = 0$, 5, 8) melts as a function of temperature. Moreover, the viscosity was measured under reduced gravity conditions to benchmark ground-based data. The self-diffusion coefficients were probed by incoherent, quasi-elastic neutron scattering. All measurements were combined with electrostatic or electromagnetic levitation, in order to process these highly reactive Titanium-based melts. From the measured density, the packing fraction was calculated as a function of temperature. In contrast to other bulk metallic glasses, the decrease in melt dynamics comes along with the decrease in packing density.

Recently, developed bulk metallic glasses (BMGs) with Sulfur have shown an improved glass forming ability (GFA) compared to their Sulfur-free counterparts.[1–3] Since Sulfur is an abundant element, which is frequently used in industry, these alloys are promising candidates for BMG production. Moreover, Sulfur incorporation allows BMG formation in Beryllium-free alloys with high Titanium contents.[1,3] Titanium-based BMGs are demanded for many industrial applications since they combine low densities, corrosion resistance, and mechanical strength.[3,4] For eutectic $Ti_{75}Ni_{25}$,[5] glass formation was reported upon Nickel substitution by Sulfur. Within this system, $Ti_{75}Ni_{17}S_8$ represents the best glass former with a critical casting thickness of 500 μm.[1] The glass transition temperature of 696 K has been detected via differential scanning calorimetry.[1] By adding Zirconium and Copper, the critical casting thickness can be enhanced up to 3 mm.[3,4] Understanding the role of Sulfur in the glass formation will allow more efficient optimization.

A complex interaction of thermophysical (e.g., density, viscosity, and self-diffusion) and thermodynamic parameters (e.g., driving force for crystallization[6–8]) controls the GFA of BMGs. However, the exact origins are still controversial.[9–12] Basically, a slowdown of melt dynamics, especially below the liquidus temperature,[13] hinders the crystallization process. One common approach to reduce the liquidus temperature is to alloy additional elements.[13–15] This can be observed, e.g., for Ni–(P), Pd–Ni–(P), and Pd–Ni–Cu–(P), where the liquidus temperature decreases toward deep eutectics with the increasing number of elements.[13] The added elements can also enhance the atomic size mismatch, which enables more efficient melt packing and leads to sluggish dynamics.[9–11] Besides that, the mixture of elements may increase the diversity of atomic bonds and create more complex crystallization paths. In terms of thermodynamics, the driving force for crystallization is a crucial parameter, which can be estimated by the Gibbs free energy difference between the solid and the liquid state.[6–8] When this difference is small, glass formation is promoted. Furthermore, a large solid/liquid interfacial energy retards crystal nucleation and, thus, favors glass formation.[9–11,16,17]

One special feature of BMGs with Sulfur is that they form a transition between metallic and chalcogenide glass formers.[1,2] In fact, molten Sulfur has a complex coordination behavior and forms many allotropes.[18] Metallic bonds are usually nondirectional and often approximated by hard spheres of defined radii.[19,20] Here, the atomic mobility is basically governed by the packing fraction.[13,15,21] For purely metallic alloys with comparable atomic radii, this approximation works quite well. Since Sulfur is a nonmetallic element, some amount

of covalent bonds could be involved as previously observed for BMGs like Zr–(Ni,Co,Cu)–Al[22–28] and Pd–Ni–P.[29] In this case, specific chemical interactions may invalidate the assumption of tabulated atomic radii.

In this study, we focus on the thermophysical properties of $Ti_{75}Ni_{25-x}S_x$ ($x = 0, 5, 8$) melts by substitution of Nickel by Sulfur. We analyzed the melt dynamics on several length scales. The macroscopic flow, characterized by viscosity, gives access to the collective motion of the atoms, while the microscopic transport, characterized by self-diffusion, describes the motion of individual atoms. Based on a hard sphere assumption with covalent radii, the relationship between packing density and melt dynamics was examined. Using containerless processing techniques, like electrostatic (ESL)[30] and electromagnetic levitation (EML),[31] these highly reactive melts were processed over broad temperature ranges.

Sample synthesis of $Ti_{75}Ni_{25-x}S_x$ ($x = 0, 5, 8$) is described in Ref. 1. To obtain samples of roughly spherical shape, portions of the master alloys were remelted in an arc furnace under a Titanium-gettered pure Argon gas atmosphere (99.9999%). The sample masses corresponded to 30–80 mg for ESL and to 0.8–1 g for EML. ESL was carried out under high-vacuum conditions of $\sim 10^{-7}$ mbar. The electrically charged samples were processed within electrostatic fields between two electrode plates. A closed feedback loop between the sample position and the side-electrode voltage kept the samples levitated.[32] Heating and melting of the samples were achieved by two infrared lasers, while a pyrometer measured the temperature without a contact. The measured temperatures were calibrated at the eutectic temperatures determined via differential scanning calorimetry. The overall uncertainty of the measured temperatures was estimated to be ± 10 K.

For density measurements,[33,34] shadow images of the samples were recorded using a high speed camera (HSC) during free radiation cooling. Under the assumption of rotational sample symmetry, an edge detection algorithm was used to calculate the pixel volume of each frame. In order to obtain absolute values of the sample volumes, a calibration with spheres of known sizes was performed. Together with the sample masses, the densities were calculated. The same setup was used for viscosity measurements via the oscillation drop technique.[34–36] Here, a sinusoidal signal was superimposed to the levitation voltage. The typical amplitude and frequency of the signal were ~ 0.3 kV and 130–200 Hz, respectively, depending on the sample mass. This superposition generates a surface oscillation. After switching off the signal, images of the samples were recorded during oscillation decay. The decay constant τ was determined by fitting the data according to $R(t) = R_0 + A \exp(-t/\tau) \sin(\omega t + \delta_0)$, where R_0 is the initial radius, A is the oscillation amplitude, ω is the frequency, and δ_0 is the phase shift. The sample viscosity was calculated based on the decay constant

$$\eta = \frac{\rho R_0^2}{5\tau}, \tag{1}$$

where ρ is the measured density. Here, a single oscillating mode of $L = 2$ and laminar flow conditions were assumed. In order to benchmark viscosity data measured on ground, EML under reduced gravity conditions was performed for $Ti_{75}Ni_{17}S_8$ during parabolic flights with the TEMPUS facility.[37] In contrast to ground-based EML, magnetic fields are sufficiently small to avoid disturbance of viscosity measurements via the oscillation drop technique.[38,39] In TEMPUS, the sample oscillation was induced by brief pulses from the heating coil. Within reduced gravity cycles of ~ 22 s, multiple oscillation decays were recorded by a HSC and sample coupling electronics (SCE).

To study the microscopic dynamics, incoherent quasi-elastic neutron scattering (QENS) was performed on the neutron time-of-flight spectrometer TOFTOF.[40] For that purpose, a mobile EML apparatus[41,42] was integrated. QENS experiments were performed under an ultra-pure Helium gas atmosphere of 700 mbar. With a neutron wavelength of 7 Å and a chopper speed of 6000 rpm, an instrumental energy resolution of 72 μeV and a wave number range of $q = 0.3 - 1.7$ Å^{-1} at zero energy transfer became accessible. The scattering law was obtained by normalizing the scattering intensity to a Vanadium standard, after background subtraction. A detailed description of the evaluation procedure is given in Ref. 43. At small wave numbers ($q < 1.0$ Å), the incoherent contributions dominate the scattering signal. In the case of $Ti_{75}Ni_{25-x}S_x$, the signal is dominated by Titanium ($\sigma_{inc.}$ (Ti) = 2.87 barn[44]) and Nickel ($\sigma_{inc.}$ (Ni) = 5.2 barn[44]) while the scattering contribution of Sulfur is rather weak ($\sigma_{inc.}$ (S) = 0.007 barn[44]).

The melt density ρ of $Ti_{75}Ni_{25-x}S_x$ ($x = 0, 5, 8$) shows a linear temperature dependence $\rho(T) = \rho_0 - \alpha T$ between 1200 and 1650 K [Fig. 1(a)], where ρ_0 is a prefactor and α is the thermal expansion coefficient. At the same time, a decrease in melt density upon Nickel substitution by Sulfur was found. Figure 1(b) shows the melt viscosity η of $Ti_{75}Ni_{25-x}S_x$ ($x = 0, 5, 8$) as a function of temperature. Within the examined temperature range of 1260 – 1680 K, an Arrhenius-type

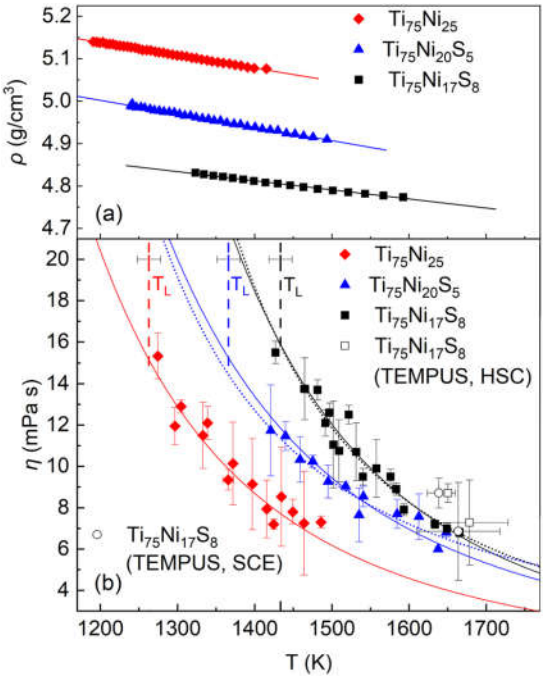

FIG. 1. (a) Melt density of $Ti_{75}Ni_{25-x}S_x$ ($x = 0, 5, 8$) as a function of temperature. An error of 1% was assumed. (b) Melt viscosity of $Ti_{75}Ni_{25-x}S_x$ ($x = 0, 5, 8$) as a function of temperature. The dashed lines indicate the liquidus temperatures, and the solid lines (dotted lines) are Arrhenius fits (VFT fits).

temperature dependence $\eta(T) = \eta_0 \exp(-E_\eta/k_B T)$ was found, where η_0 is a prefactor, E_η the activation energy of viscosity, and k_B the Boltzmann constant. The fit parameters for the linear temperature dependence of the density and the Arrhenius-type temperature dependence of the viscosity are given in Table I. In order to compare our viscosity data with those of other alloy systems, the Vogel–Fulcher–Tammann (VFT) fit parameters with an assumed viscosity of 10^{12} Pa s at glass transition temperature[6] are also shown for $Ti_{75}Ni_{25-x}S_x$ ($x = 5, 8$). Due to the onset of crystallization upon heating, the glass transition temperature of $Ti_{75}Ni_{20}S_5$ is not detectable in differential scanning calorimetry measurements.[3] In order to get a rough estimate of the fragility parameter also for this alloy, the glass transition temperature of $Ti_{75}Ni_{17}S_8$ was used for both VFT fits [Fig. 1(b)].

The replacement of Nickel by Sulfur leads to an increase in the melt viscosity at equal temperatures. For example, at 1447 K, the melt viscosity of $Ti_{75}Ni_{25}$ corresponds to 7.1 mPa s. For $Ti_{75}Ni_{20}S_5$, the melt viscosity increases to 11.0 mPa s and for $Ti_{75}Ni_{17}S_8$ to 15.0 mPa s. Hence, the viscosity of $Ti_{75}Ni_{17}S_8$ is more than twice as large as the one of $Ti_{75}Ni_{25}$ at the same temperature. This trend becomes clearer with decreasing temperature. At the liquidus temperatures, all alloys show comparable viscosities. From ESL and synchrotron experiments, an increase in the liquidus temperature upon Sulfur incorporation was found. At the same time, the solidus temperature obtained from differential scanning calorimetry decreases. Therefore, the two phase field between solidus and liquidus temperature expands with the increasing Sulfur content. The TEMPUS data [Fig. 1(b)] agree with the ESL viscosity data within the experimental uncertainty.

TABLE I. Parameters obtained from linear, Arrhenius, and VFT fits of the melt density, melt viscosity, and self-diffusion, respectively, for $Ti_{75}Ni_{25-x}S_x$ ($x = 0, 5, 8$).

Linear ρ	x	ρ_0 (g/cm^3)	α (10^{-4}g/cm^{3}K^1)	
	0	5.501 ± 0.001	3.02 ± 0.01	
	5	5.382 ± 0.003	3.17 ± 0.02	
	8	5.112 ± 0.003	2.14 ± 0.02	
Arrhenius η	x	η_0 (mPa s)	E_η (eV)	
	0	0.05 ± 0.02	0.62 ± 0.05	
	5	0.07 ± 0.02	0.63 ± 0.04	
	8	0.03 ± 0.01	0.77 ± 0.04	
VFT η	x	η_0 (mPa s)	D^*	T_0 (K)
	5	0.79 ± 0.02	3.46 ± 0.37	623 ± 5
	8	0.31 ± 0.01	5.61 ± 0.47	592 ± 6
Arrhenius D	x	D_0 (10^{-7} m^2 s^{-1})	E_D (eV)	
	0	2.18 ± 0.07	0.56 ± 0.04	
	5	3.31 ± 0.05	0.66 ± 0.02	

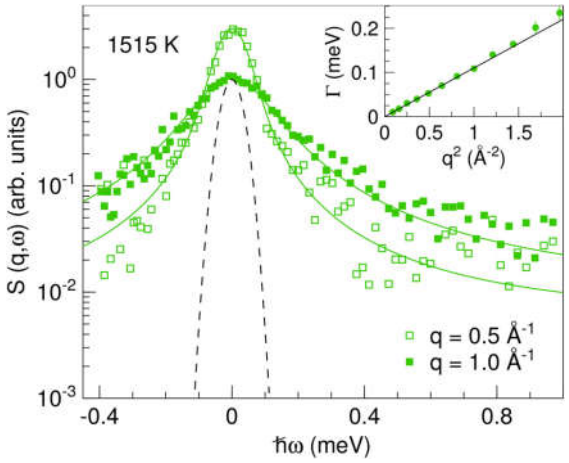

FIG. 2. Scattering laws for $Ti_{75}Ni_{17}S_8$ at 1515 K with $q = 0.5$ Å^{-1} and $q = 1$ Å^{-1}. The solid lines represent Lorentzian fits, and the dashed line represents the instrumental resolution function. The inset shows the full-width-at-half-maximum of the Lorentzian fits against q^2. The solid line represents a linear fit.

Figure 2 shows the scattering laws for $Ti_{75}Ni_{17}S_8$ at 1515 K with $q = 0.5$ Å^{-1} and $q = 1.0$ Å^{-1}, fitted by single Lorentzian functions convoluted with the instrumental resolution function. Below 1.0 Å^{-2}, a linear q^2 dependence was found for the full-width-at-half-maximum of the Lorentzian fits. The slope corresponds to the self-diffusion coefficient

$$D = \Gamma/\hbar q^2, \tag{2}$$

where Γ is the full-width-at-half-maximum. Since a single Lorentzian function describes each scattering law sufficiently, the self-diffusion coefficients of Titanium and Nickel should be comparable.[45] Figure 3 shows the mean Ti/Ni self-diffusion coefficients of $Ti_{75}Ni_{25-x}S_x$ ($x = 0$, 5, 8) as a function of temperature. At 1000/T = 0.69 (1447 K), the

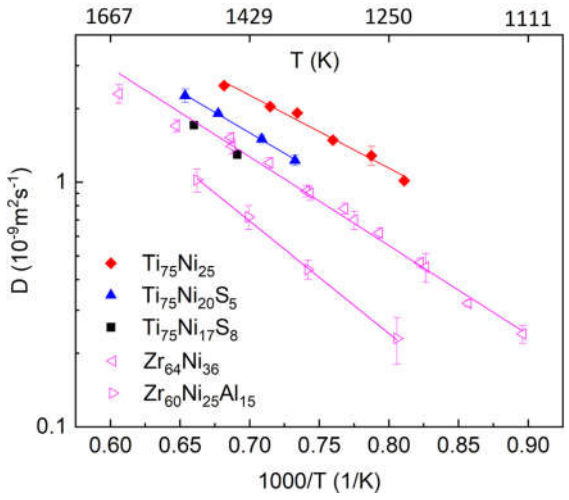

FIG. 3. Mean Ti/Ni self-diffusion coefficients of $Ti_{75}Ni_{25-x}S_x$ ($x = 0, 5, 8$) as a function of inverse temperature. For comparison, the Ni self-diffusion coefficients of $Zr_{60}Ni_{25}Al_{15}$[25] and $Zr_{64}Ni_{36}$[34] are shown. The solid lines represent Arrhenius fits.

binary alloy exhibits the highest mean Ti/Ni self-diffusion coefficient of 2.4×10^{-9} m^2 s^{-1}, followed by $Ti_{75}Ni_{20}S_5$ with 1.7×10^{-9} m^2 s^{-1} and $Ti_{75}Ni_{17}S_8$ with 1.3×10^{-9} m^2 s^{-1}. Basically, we observe the same trend of reduced melt dynamics as previously reported for the viscosity. In addition, literature data for $Zr_{60}Ni_{25}Al_{15}$[25] and $Zr_{64}Ni_{36}$[34] are shown. The Ni self-diffusion of $Zr_{64}Ni_{36}$ is similar to the mean Ti/Ni self-diffusion of $Ti_{75}Ni_{17}S_8$, while the Ni self-diffusion for $Zr_{60}Ni_{25}Al_{15}$ is one order of magnitude lower. An Arrhenius-type temperature dependence $D(T) = D_0 \exp(-E_D/k_B T)$ was found for $Ti_{75}Ni_{25-x}S_x$ ($x = 0, 5$) (Table I), where D_0 is a prefactor and E_D the activation energy of self-diffusion. The activation energy of both alloys is higher than the one for pure Nickel.[46] $Ti_{75}Ni_{20}S_5$ shows comparable values to $Zr_{64}Ni_{36}$, while the activation energy for $Zr_{60}Ni_{25}Al_{15}$ is slightly higher.[24]

To confirm if the slowdown of the melt dynamics is connected to dense packing, the packing fraction was calculated in the framework of hard sphere assumption with covalent radii [$r(Ti)_{cov.} = 1.324$ Å; $r(Ni)_{cov.} = 1.149$ Å; and $r(S)_{cov.} = 1.04$ Å[47]]. During the first calculation step, number density n was determined,

$$n = \frac{\rho N_a}{\bar{M}}, \tag{3}$$

where ρ is the melt density, N_a the Avogadro constant, and $\bar{M}$ is the average molar mass. With the number density, packing fraction φ was calculated

$$\varphi = \bar{V} n, \tag{4}$$

where $\bar{V}$ is the weighted mean atomic volume of the hard spheres. Figure 4 shows the packing fraction and the number density of $Ti_{75}Ni_{25-x}S_x$ ($x = 0, 5, 8$) melts as a function of temperature. We observe a decrease in the packing fraction with the increasing Sulfur content. While the packing fraction depends on the assumed atomic radii, the number density simply depends on the measured density. However, we observe that $Ti_{75}Ni_{17}S_8$ exhibits a smaller number density than the alloys with a lower Sulfur content.

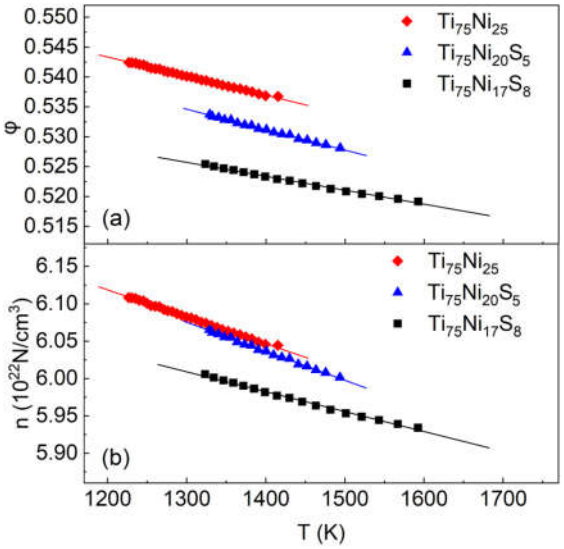

FIG. 4. (a) Packing fraction of $Ti_{75}Ni_{25-x}S_x$ ($x = 0, 5, 8$) calculated from density as a function of temperature. An error of 1% was determined. (b) Number density of $Ti_{75}Ni_{25-x}S_x$ ($x = 0, 5, 8$) calculated from density as a function of temperature. An error of 1% was determined.

The slowdown of melt dynamics cannot be explained by a suitable choice of deep eutectic composition since the liquidus temperature increases upon Sulfur incorporation. Moreover, all analyzed alloys show comparable viscosities at their liquidus temperatures, which do not reflect their different GFA. By adding small Sulfur atoms, a more efficient melt packing was expected due to the atomic size mismatch. However, this consideration is refuted since the packing fraction decreases upon Nickel substitution by Sulfur. While the number density remains nearly constant with 5 at. % Sulfur, it decreases with 8 at. % Sulfur. This observation indicates that Sulfur may occupy a larger space in the melt structure than the one assumed for hard spheres with covalent radii. A decrease in packing density in combination with reduced melt dynamics was previously reported for Aluminum addition in Zr–(Ni,Co) melts due to specific chemical interactions between Aluminum and the transition metals.[25] A similar origin may be considered for the sluggish dynamics observed here.

In conclusion, we determined the density, the viscosity, and the self-diffusion of $Ti_{75}Ni_{25-x}S_x$ ($x = 0, 5, 8$) melts over broad temperature ranges by applying levitation techniques. The GFA enhancement upon Sulfur addition can be explained neither by a reduction of the liquidus temperature nor by dense packing of hard spheres. The decrease in melt dynamics comes along with a decrease in melt packing, which may indicate covalent interactions involved. The unique melt structure should be subjected to further analysis.

We acknowledge M. Wolf from the Heinz Maier Leibnitz Zentrum (MLZ), Technical University of Munich, and E. Sondermann, T. Aumüller, and T. Schiller from the Institute of Materials Physics in Space, German Aerospace Center (DLR), for their assistance during the beam time at TOFTOF. We also thank the TEMPUS crew for their technical support during the parabolic flight campaign. For financial support, we gratefully acknowledge the German Research Foundation (DFG) through the grants (No. ME 1958/12-1 and BU 2276/11-1).

DATA AVAILABILITY

The data that support the findings of this study are available from the corresponding author upon reasonable request.

REFERENCES

[1] A. Kuball, O. Gross, B. Bochtler, and R. Busch, Scr. Mater. **146**, 73 (2018).
[2] A. Kuball, B. Bochtler, O. Gross, V. Pacheco, M. Stolpe, S. Hechler, and R. Busch, Acta Mater. **158**, 13 (2018).
[3] A. Kuball, O. Gross, B. Bochtler, B. Adam, L. Ruschel, M. Zamanzade, and R. Busch, J. Alloys Compd. **790**, 337 (2019).
[4] O. Gross, L. Ruschel, A. Kuball, B. Bochtler, B. Adam, and R. Busch, J. Phys.: Condens. Matter **32**, 264003 (2020).
[5] J. E. Garay, U. Anselmi-Tamburini, and Z. A. Munir, Acta Mater. **51**, 4487 (2003).
[6] R. Busch, J. Miner., Met. Mater. Soc. **52**, 39 (2000).
[7] R. Busch, J. Schroers, and W. H. Wang, Mrs Bull. **32**, 620 (2007).
[8] R. Busch and I. Gallino, J. Miner., Met. Mater. Soc. **69**, 2178 (2017).
[9] A. Inoue, Mater. Trans., JIM **36**, 866 (1995).
[10] A. Inoue, Acta Mater. **48**, 279 (2000).
[11] A. Inoue and A. Takeuchi, Mater. Sci. Eng., A **375–377**, 16 (2004).

[12]W. H. Wang, C. Dong, and C. H. Shek, Mater. Sci. Eng., R **44**, 45 (2004).
[13]S. M. Chathoth, A. Meyer, M. M. Koza, and F. Juranyi, Appl. Phys. Lett. **85**, 4881 (2004).
[14]Z. P. Lu and C. T. Liu, J. Mater. Sci. **39**, 3965 (2004).
[15]S. M. Chathoth, B. Damaschke, M. M. Koza, and K. Samwer, Phys. Rev. Lett. **101**, 037801 (2008).
[16]D. R. Nelson and F. Spaepen, in *Solid State Physics* (Elsevier, 1989), Vol. 42, pp. 1–90.
[17]D. Holland-Moritz, Int. J. Non-Equilib. Process. **11**, 169 (1998).
[18]R. Bellissent, L. Descotes, F. Boué, and P. Pfeuty, Phys. Rev. B **41**, 2135 (1990).
[19]J. Bernal, Nature **185**, 68 (1960).
[20]H. Sheng, W. Luo, F. Alamgir, J. Bai, and E. Ma, Nature **439**, 419 (2006).
[21]S. M. Chathoth, Europhys. Lett. **95**, 26001 (2011).
[22]E. Matsubara, T. Tamura, Y. Waseda, A. Inoue, T. Zhang, and T. Masumoto, Mater. Trans., JIM **33**, 873 (1992).
[23]Y. Q. Cheng, E. Ma, and H. W. Sheng, Phys. Rev. Lett. **102**, 245501 (2009).
[24]D. Holland-Moritz, S. Stüber, H. Hartmann, T. Unruh, and A. Meyer, J. Phys.: Conf. Ser. **144**, 012119 (2009).
[25]C. C. Yuan, F. Yang, F. Kargl, D. Holland-Moritz, G. G. Simeoni, and A. Meyer, Phys. Rev. B **91**, 214203 (2015).
[26]S. W. Basuki, F. Yang, E. Gill, K. Rätzke, A. Meyer, and F. Faupel, Phys. Rev. B **95**, 024301 (2017).
[27]H. L. Peng, F. Yang, S. T. Liu, D. Holland-Moritz, T. Kordel, T. Hansen, and T. Voigtmann, Phys. Rev. B **100**, 104202 (2019).
[28]C. C. Yuan, F. Yang, X. K. Xi, C. L. Shi, D. Holland-Moritz, M. Z. Li, F. Hu, B. L. Shen, X. L. Wang, A. Meyer *et al.*, Mater. Today **32**, 26 (2020).
[29]P. F. Guan, T. Fujita, A. Hirata, Y. H. Liu, and M. W. Chen, Phys. Rev. Lett. **108**, 175501 (2012).
[30]W.-K. Rhim, S. K. Chung, D. Barber, K. F. Man, G. Gutt, A. Rulison, and R. E. Spjut, Rev. Sci. Instrum. **64**, 2961 (1993).
[31]E. Okress, D. Wroughton, G. Comenetz, P. Brace, and J. Kelly, J. Appl. Phys. **23**, 545 (1952).
[32]T. Meister, *Aufbau Und Regelung Eines Elektrostatischen Levitators* (VDI-Verlag, 2001).
[33]J. Brillo and I. Egry, Int. J. Thermophys. **24**, 1155 (2003).
[34]J. Brillo, A. I. Pommrich, and A. Meyer, Phys. Rev. Lett. **107**, 165902 (2011).
[35]W.-K. Rhim, K. Ohsaka, P.-F. Paradis, and R. E. Spjut, Rev. Sci. Instrum. **70**, 2796 (1999).
[36]P. Heintzmann, F. Yang, S. Schneider, G. Lohöfer, and A. Meyer, Appl. Phys. Lett. **108**, 241908 (2016).
[37]G. Lohöfer and J. Piller, in 40th AIAA Aerospace Sciences Meeting and Exhibit (2002), p. 764.
[38]I. Egry, G. Lohöfer, I. Seyhan, S. Schneider, and B. Feuerbacher, Appl. Phys. Lett. **73**, 462 (1998).
[39]I. Egry, G. Lohöfer, I. Seyhan, S. Schneider, and B. Feuerbacher, Int. J. Thermophys. **20**, 1005 (1999).
[40]W. Lohstroh and Z. Evenson, J. Large-Scale Res. Facil. **1**, 15 (2015).
[41]D. Holland-Moritz, T. Schenk, P. Convert, T. Hansen, and D. M. Herlach, Meas. Sci. Technol. **16**, 372 (2005).
[42]D. Holland-Moritz, S. Stüber, H. Hartmann, T. Unruh, T. Hansen, and A. Meyer, Phys. Rev. B **79**, 064204 (2009).
[43]A. Meyer, *EPJ Web Conf.* **83**, 01002 (2015).
[44]V. F. Sears, Neutron News **3**, 26 (1992).
[45]Beside the incoherent scattering contributions from Titanium and Nickel, the negative scattering length of Titanium may involve some coherent scattering constitutions. Nevertheless, these coherent scattering contributions do not significantly affect the value of the obtained selfdiffusion coefficients.
[46]A. Meyer, S. Stüber, D. Holland-Moritz, O. Heinen, and T. Unruh, Phys. Rev. B **77**, 092201 (2008).
[47]L. Pauling, J. Am. Chem. Soc. **69**, 542 (1947).